EFFECTS OF FREE-STREAM TURBULENCE ON TURBULENT BOUNDARY LAYER SUBJECTED TO ADVERSE PRESSURE GRADIENT

Tomoya Houra
Department of Environmental Technology,
Nagoya Institute of Technology,
Gokiso-cho, Showa-ku, Nagoya 466-8555, Japan
houra@heat.mech.nitech.ac.jp

Yasutaka Nagano
Department of Mechanical Engineering,
Nagoya Institute of Technology,
Gokiso-cho, Showa-ku, Nagoya 466-8555, Japan
nagano@heat.mech.nitech.ac.jp

ABSTRACT

We have investigated the effects of free-stream turbulence on a turbulent boundary layer developing on a flat plate with and without streamwise pressure gradient. An active type turbulence grid located in the settling chamber is used to generate the free-stream turbulence; its intensity is about 1%, and the length scale is about 1.0 times the boundary layer thickness. Despite the slight increase in the streamwise turbulence intensity at the outer edge of the boundary layer, the intensity becomes much larger in the middle of the layer, and these tendencies are more evident in an adverse-pressure-gradient flow. The absolute value of the third-order moment $\overline{vuv}$ in the outer region increases remarkably in the adverse-pressure-gradient flow with free-stream turbulence. Thus, the wallward transfer observed in the adverse-pressure-gradient flow is enhanced by imposing free-stream turbulence. Moreover the local wavelet spectra reveal that a strong interaction, consisting of the near-wall turbulence with high frequency and free-stream turbulence with low frequency, occurs intermittently.

INTRODUCTION

Interaction between wall-bounded shear flow and free shear flow is an important issue to assess the turbulence theory and existing turbulence models. Previous experimental studies (Hancock and Bradshaw, 1983; Blair, 1983; Castro, 1984) have revealed that the effects of free-stream turbulence (FST) depend significantly on both the free-stream intensity and the length scale ratio between the boundary layer and external free-stream. For the prediction of the increase in the skin friction, the empirical correlation is provided in conjunction with the length-scale correction. On the other hand, for the heat transfer, this correction is not suitable, and a more rational correction should be provided (Baskaran *et al.*, 1989). Moreover, for the real situation in fluid machinery, such as a diffuser and turbine blades, the mean velocity variation in the free-stream, i.e., streamwise pressure gradients, should be considered as well as the free-stream turbulent properties. The combined effects of the free-stream turbulence and the pressure gradients on the turbulent structures have not been fully discussed so far.

In this study, we have experimentally investigated the effects of FST and the adverse pressure gradient (APG) on the turbulent boundary layer developing along a flat plate. An active turbulence grid located in the settling chamber is used to generate the free-stream turbulence; its intensity and length scale are about 1% and 1.0 δ (boundary layer thickness at the measurement location), respectively.

EXPERIMENTAL APPARATUS

The experimental apparatus used is the same as described in our previous studies (Nagano *et al.*, 1993, 1998; Houra *et al.*, 2000). The turbulence generating grid is installed in the settling chamber located upstream of the test section. To generate the free-stream turbulence, we adopted the active type grid specially devised for the present measurement as shown in Fig. 1. The active grid is composed of 13 horizontal and 8 vertical rotating shafts to which triangle-shaped winglets are attached. The shafts are made of 10 mm aluminum pipe. Along each shaft, the 23 $\times$ 46 mm^2 right triangle-shaped winglets of 0.1 mm-thick aluminum plate are attached to both sides. The horizontal and vertical shafts have 9 and 14 pairs of winglets, respectively, so that the grid size, M, is 50 mm. Each shaft is independently driven by a 7.2 W DC motor (Japan Servo Co., Ltd., DME37BA). The control signals are generated by a PC and sent to the driver circuits through the USB port. Each motor is set to a fixed rotational speed of 490 r.p.m. in one direction.

Velocity measurement was done with hot-wire probes, i.e., a handmade subminiature (Ligrani and Bradshaw, 1987) normal hot-wire (diameter: 3.1 μm; length: 0.6 mm), and a specially

Table 1: Flow parameters (x = 525 mm, $\overline{U}_0$=11.0 m/s)

	$\overline{U}_e$ [m/s]	u_τ [m/s]	δ [mm]	R_θ	P^+ $\times 10^2$	β	Tu [%]	L_e/δ
ZPG	11.0	0.528	12.0	1200	0	0	0	-
	11.0	0.536	16.3	1420	0	0	1.0	1.0
APG	9.5	0.410	17.0	1620	8.4	0.84	0	-
	9.4	0.420	20.8	1530	7.2	0.71	1.1	0.8

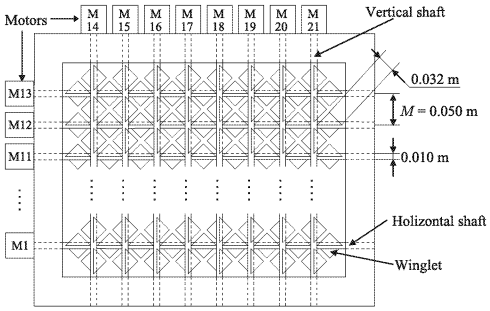

Figure 1: Schematic of the active grid

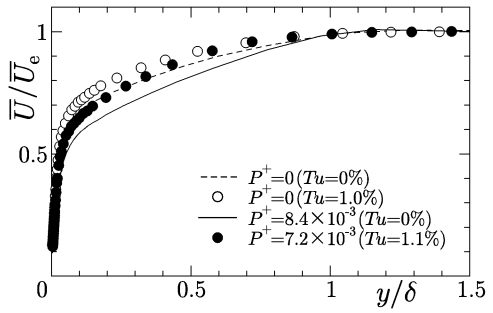

Figure 2: Mean velocity profiles in outer coordinate.

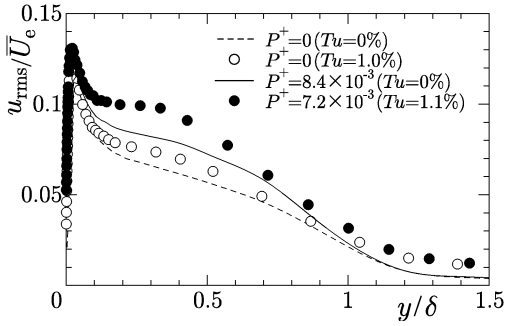

Figure 3: Turbulence intensities of streamwise velocity fluctuation in outer coordinate.

devised X-probe, which is composed of two symmetrically bent V-shaped hot wires (Hishida and Nagano, 1988) for measurement of two velocity components in the streamwise (x) and wall-normal (y) directions (diameter: 5 μm; length of each side: 0.4 mm $\simeq$ 5 ν/u_τ; and spacing: 0.30 mm $\simeq$ 3.8 ν/u_τ).

The important parameters in the flow field of the present measurement are listed in Table 1. In the APG flow, the pressure gradient dC_p/dx [$C_p = (\overline{P}-\overline{P}_0)/(\rho\overline{U}_0^2/2)$, and $\overline{P}$, $\overline{P}_0$ and $\overline{U}_0$ are the mean pressure, the reference inlet pressure, and the reference inlet velocity, respectively] keeps a nearly constant value of 0.6 m^{-1} over the region 65 mm $\leq x \leq$ 700 mm, and then decreases slowly (x is the streamwise distance from a tripping point). On the other hand, the pressure gradient parameter normalized by inner variables P^+ [$= \nu(d\overline{P}/dx)/\rho u_\tau^3$] and the Clauser parameter β [$= (\delta^*/\tau_w)\, d\overline{P}/dx$] increase with increasing x, thus yielding moderate to strong APG.

The free-stream turbulence intensity Tu is defined as the ratio between the r.m.s. intensity of streamwise velocity fluctuation to the streamwise mean velocity in the free-stream. The length scale in the free-stream is estimated as follows, using the assumptions of the local isotropy and Taylor's frozen turbulence:

$$L_e = k^{\frac{3}{2}}/\varepsilon \simeq (3\,\overline{u^2}/2)^{\frac{3}{2}} \left[15\,\nu\,\overline{(\partial u/\partial x)^2}\right]^{-1} \simeq (3\,\overline{u^2}/2)^{\frac{3}{2}} \left[15\,\nu\,\overline{(\partial u/\partial t)^2}/\overline{U}^2\right]^{-1}. \quad (1)$$

RESULTS AND DISCUSSION

Mean velocity and turbulent intensities

Figures 2 and 3 respectively show the mean velocity $\overline{U}$ and the r.m.s. intensity of the streamwise component $u_{\rm rms}$ normalized by the free-stream velocity $\overline{U}_e$. The abscissa is the distance from the wall normalized by the 99% thickness of the boundary layer δ. As seen from Fig. 2, the defect in the mean velocity $\overline{U}$ from the free-stream velocity $\overline{U}_e$ becomes larger in the near-wall region in the APG flow than in the ZPG flow. Under the influence of the FST, the boundary layer thickness δ grows rapidly, irrespective of the pressure gradient. Moreover, the mean velocity increases at the same wall-normal distance y/δ. On the other hand, as seen from Fig. 3, despite the slight increase in the turbulence intensity at the outer edge of the boundary layer, the intensity becomes much larger in the middle of the layer, and these tendencies are more evident in the APG flow. This might be because large-scale sweep motions from the outer to the inner regions predominate in the APG flow (Houra *et al.*, 2000).

Figure 4 shows the mean velocity profiles normalized by the friction velocity u_τ. As clearly seen from this figure, the velocity profiles in APG flows lie below the following 'standard' log-law profile for ZPG flows:

$$\overline{U}^+ = 2.44 \ln y^+ + 5.0. \quad (2)$$

In the outer region, the wake components of the mean velocity profiles are enhanced by imposing APG. However, the FST reduces the wake components in both the ZPG and APG flows.

The intensity profiles of the fluctuating velocity components, u and v, normalized by u_τ, are presented in Figs. 5(a) and 5(b), respectively. In the APG flow, both of the velocity fluctuation components become large in the outer region. The profiles of the Reynolds shear stress in the wall coordinate also increase in the outer region (not shown here). This means that the viscous wall unit cannot be used to describe the feature of the non-equilibrium APG flows (Nagano *et al.*, 1993, 1998). With increasing the FST, $u_{\rm rms}$ increases outside the buffer region. On the other hand, $v_{\rm rms}$ scarcely increases except at the outer edge of the boundary layer, where $v_{\rm rms}$ is larger than $u_{\rm rms}$ due to the effects of the contraction located downstream of the active grid (Batchelor, 1953; the present contraction ratio is 9:1) in the settling chamber.

Turbulent transports

There is little knowledge of what effects the APG and FST produce on the higher-order turbulence statistics. Since the structural differences in quasi-coherent motions reflect on higher-order turbulence statistics, especially third-order mo-

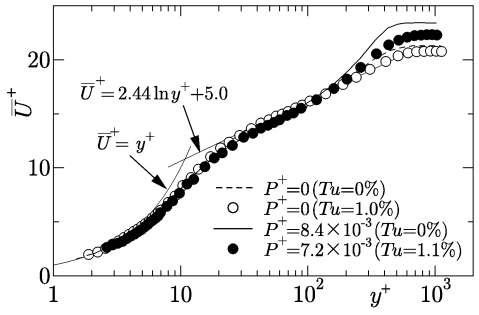

Figure 4: Mean velocity profiles in wall coordinate.

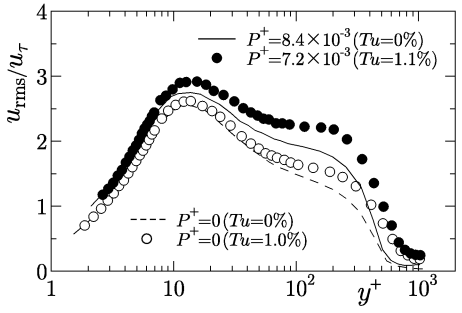

(a) Streamwise

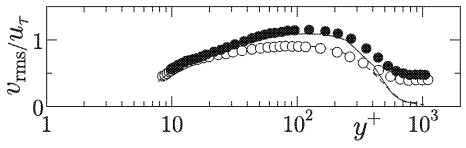

(b) Wall-normal

Figure 5: Turbulence intensities in wall coordinate.

ments (Nagano and Tagawa, 1988), it is very important to investigate these moments. Figure 6 shows the time-averaged turbulent transport of the Reynolds shear stress normalized by the friction velocity u_τ. Definite effects of the APG and FST are clearly seen on the third-order moment. In the APG flow without the FST, the absolute value of $\overline{vuv}/u_\tau^3$ decreases in the log region and increases in the outer region compared with that in the ZPG flow without the FST (see solid and broken lines in Fig. 6). The definite change of $\overline{vuv}$ in the near-wall to outer regions demonstrate the existence of turbulent transport of the Reynolds shear stress toward the wall from the regions away from the wall. This important characteristic of the APG flow conforms to our previous results (Nagano *et al.*, 1993; Houra *et al.*, 2000), and is also consistent with the results of Bradshaw (1967), Cutler and Johnston (1989), and Skåre and Krogstad (1994).

On the other hand, if the FST is imposed on the flow field, the FST effect is very small in the inner region. However, in the outer region, the absolute value of $\overline{vuv}$ increases remarkably in the APG flow with the FST. Thus, the wallward transfer observed in the APG flow is enhanced by imposing the FST.

Fractional contributions

The fractional contributions of different quadrant motions to $\overline{vuv}$, normalized by the friction velocity u_τ, are shown in

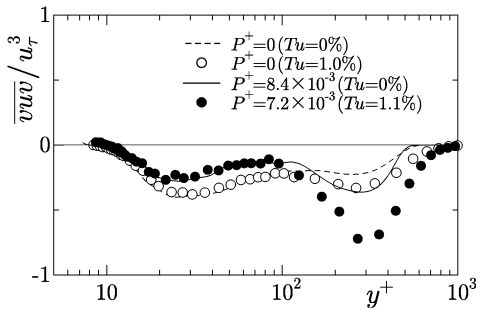

Figure 6: Profiles of turbulence transport in wall coordinate.

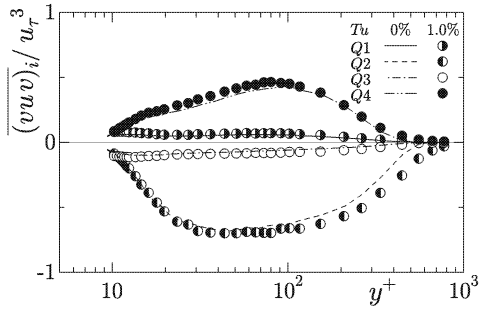

(a) ZPG flows

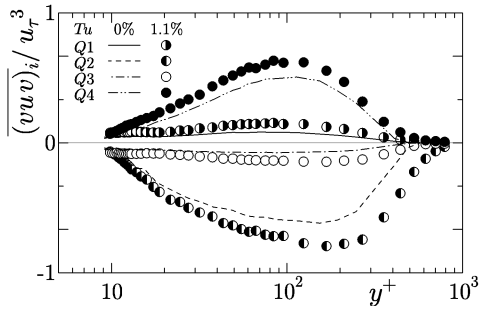

(b) APG flows

Figure 7: Fractional contributions of different quadrant motions to the third-order moment $\overline{vuv}$.

Fig. 7. In the ZPG flow, as is apparent from Fig. 7(a), the turbulent transport of uv in the wall-normal direction is dominated mainly by the $Q2$- and $Q4$-motions. Since the net values of the triple products are determined by the disparity in contributions between these two types of motions, $\overline{vuv}$ result in negative value outside the buffer region of the ZPG flows where the ejections ($Q2$) become larger than the sweeps ($Q4$).

In the APG flow without the FST, as shown in Fig. 7(b), the contributions from the coherent motions, especially the ejections ($Q2$), significantly decrease in the log region. Thus, the triple product $\overline{vuv}$ in the log region of the APG flow have net values smaller than those in the ZPG flow. On the other hand, if the FST is imposed, all of the quadrant motions are enhanced in the APG flow [see symbols in Fig. 7(b)]. Moreover, the absolute value of the contribution from the $Q2$-motions is much enhanced in the outer region. Thus, the net value of the $\overline{vuv}$ becomes larger in the outer region as shown in Fig. 6.

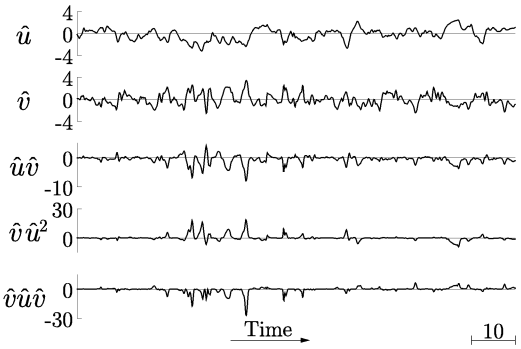

(a) $P^+ = 8.4 \times 10^{-3} (Tu = 0\%)$

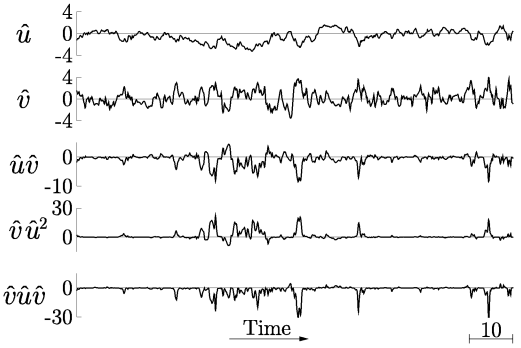

(b) $P^+ = 7.2 \times 10^{-3} (Tu = 1.1\%)$

Figure 8: Simultaneous signal traces of third-order moments $\hat{v}\hat{u}^2$ and $\hat{v}\hat{u}\hat{v}$ in APG flows ($y^+ \simeq 300$).

Instantaneous characteristics of turbulence quantities

To understand the above features of the APG flows in more detail, we have investigated the instantaneous characteristics of the coherent motions. Figures 8 show the instantaneous signals of uv, vu^2 and vuv together with u- and v-fluctuations at $y^+ \simeq 300$, where the time-averaged values of triple product $\overline{vuv}$ become nearly maximum in the APG flow with the FST (see Fig. 6). In this figure, a circumflex " ˆ " denotes the normalization by the respective r.m.s. value. The time on the abscissa is normalized by the Taylor time scale τ_E $\left[= \sqrt{2\,\overline{u^2}/\overline{(\partial u/\partial t)^2}}\right]$, which is the most appropriate for scaling the period of the coherent motions, irrespective of pressure gradients (Nagano *et al.*, 1998; see also Fig. 10). The mean burst periods have nearly 10 τ_E in APG flows at this location.

As seen from Fig. 8(a), the large amplitude fluctuation from the $Q2$-motions is observed in this location. If the FST is imposed [Fig. 8(b)], the contribution from the large amplitude $Q2$-motions occurs more frequently. In the canonical wall flows, the u-fluctuation contains lower frequency motions, whereas the v-fluctuation contains higher frequency motions. These disparities in the frequency become larger by imposing the FST. The intermittent signals of third-order moments, vu^2 and vuv, contain the higher frequency fluctuations.

Time scales and spectra of velocity fluctuations

Next, to investigate the relationship between the scales of the FST and that of the boundary layer, Figs. 9 and 10 show the integral time scale T_E and the Taylor time scale τ_E, respectively. These time scales are normalized with the constant free-stream velocity at the inlet to the test section $\overline{U}_0$ and kinematic viscosity ν, to clarify the quantitative change in the profiles. As seen from Fig. 9, under the influence of the FST, the integral time scale strikingly increases in the entire region of both ZPG and APG flows. On the other hand, the Taylor time scale τ_E also increases as shown in Fig. 10; however, its increments are relatively small compared to those of the integral time scale.

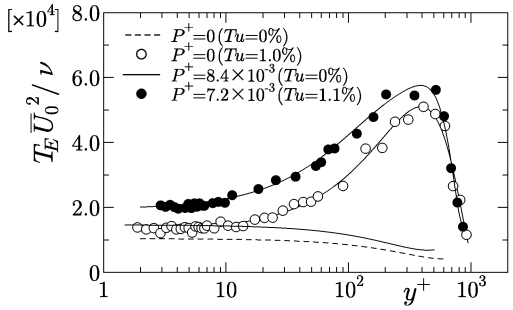

Figure 9: Distributions of integral time scale.

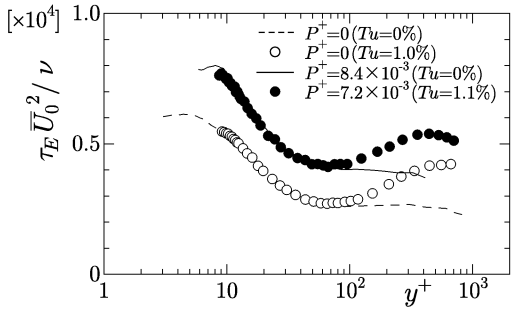

Figure 10: Distributions of Taylor time scale.

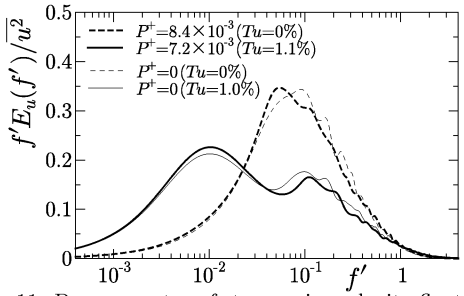

Figure 11: Power spectra of streamwise velocity fluctuation in the outer layer ($y^+ \simeq 300$).

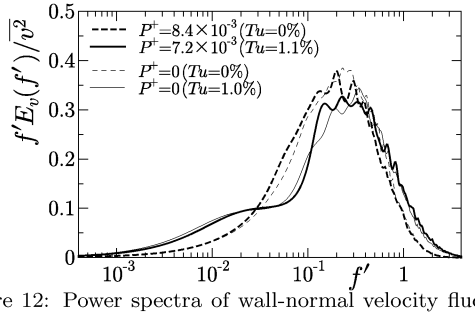

Figure 12: Power spectra of wall-normal velocity fluctuation in the outer layer ($y^+ \simeq 300$).

Next, Figs. 11 and 12 show the power spectra of the streamwise and wall-normal velocity fluctuations in the outer layer ($y^+ \simeq 300$). The abscissa is frequency normalized by the

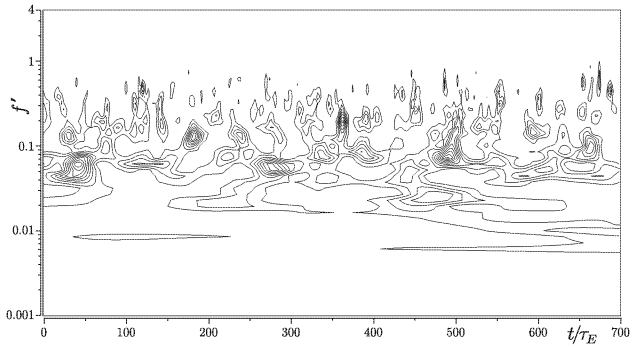

(a) $E_{uu}(a', t/\tau_E)/\left(a' C_\psi \overline{u^2}\right)$

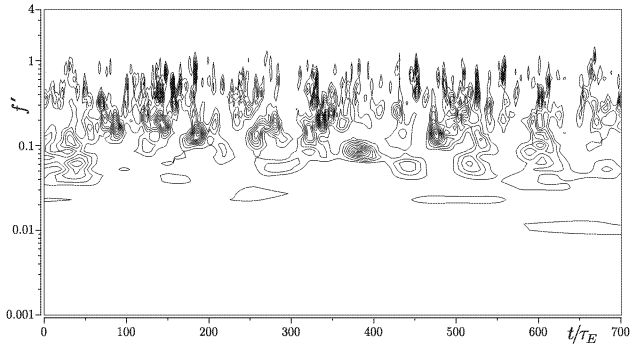

(b) $E_{vv}(a', t/\tau_E)/\left(a' C_\psi \overline{v^2}\right)$

Figure 13: Wavelet scalograms of velocity fluctuations in the outer layer ($P^+ = 8.4 \times 10^{-3}, Tu = 0\%, y^+ \simeq 300$).

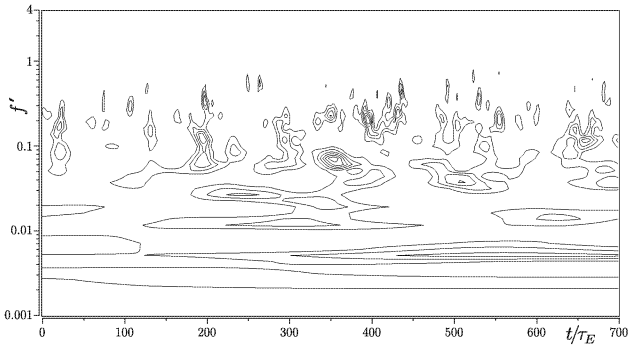

(a) $E_{uu}(a', t/\tau_E)/\left(a' C_\psi \overline{u^2}\right)$

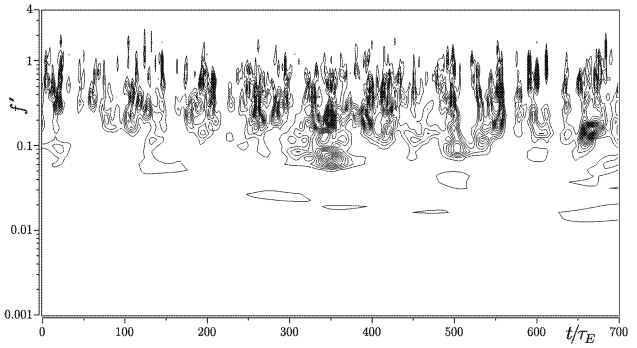

(b) $E_{vv}(a', t/\tau_E)/\left(a' C_\psi \overline{v^2}\right)$

Figure 14: Wavelet scalograms of velocity fluctuations in the outer layer ($P^+ = 7.2 \times 10^{-3}, Tu = 1.1\%, y^+ \simeq 300$).

Taylor time scale, $f' = f\,\tau_E$. As seen from Figs. 11 and 12, the arranged spectra with the Taylor time scale are well correlated irrespective of the pressure gradient without the FST, thus indicating the validation of the scaling with the Taylor time scale (Nagano *et al.*, 1998). By imposing the FST, the spectra of streamwise velocity fluctuations have two peaks: the higher one is the contribution from the turbulent structures embedded in the boundary layer, while the lower is from the free-stream turbulence generated by the grid. In the near-wall region, inside the buffer layer, the contribution to the power spectra from lower frequency cannot be seen (not shown here). Surprisingly, the spectra of streamwise velocity fluctuation with and without the FST also well correlated in the higher frequency region as shown in the Fig. 11. On the other hand, for the wall-normal velocity fluctuations, although the contribution from the lower frequency is small, the v-fluctuation contains the energy in the higher frequency region than without the FST as shown Fig. 12.

Wavelet analysis of turbulent signals

Finally, to investigate the local relation between the position and scale of the turbulent signals, we analyzed the same signals shown in Figs. 8(a) and 8(b) using the continuous wavelet transform. The one-dimensional continuous wavelet transform of time-series data $X(t)$ is defined (e.g., Farge *et al.*, 1996; Nagano and Houra, 2002) as

$$W_X(a,t) = \frac{1}{\sqrt{|a|}} \int_{-\infty}^{\infty} X(t')\,\psi^*\left(\frac{t'-t}{a}\right) dt' \qquad (3)$$

where $\psi(t)$ is an analyzing wavelet, * denotes the complex conjugate, and a is the scaling parameter. As the analyzing wavelet, we adopted the Morlet wavelet,

$$\psi(t) = e^{i2\pi k_\psi t} e^{-t^2/2}, \qquad (4)$$

whose Fourier transform is

$$\hat{\psi}(f) = \sqrt{2\pi}\, e^{-[2\pi(f-k_\psi)]^2/2}. \qquad (5)$$

If we put $k_\psi = 1$, the scaling parameter, a, corresponds to the inverse of the frequency as $a = 1/f$. Although the Morlet wavelet does not satisfy the following admissibility condition

$$C_\psi = \int_{-\infty}^{+\infty} \frac{|\hat{\psi}(f)|^2}{|f|}\, df < \infty, \qquad (6)$$

we used the empirical approximation and estimated the admissibility constant, C_ψ, for the Morlet wavelet,

$$C_\psi = \int_{-\infty}^{\infty} |\hat{\psi}(f)|^2/|f|\, df \simeq \int_{-\infty}^{\infty} |\hat{\psi}(f)|^2\, df = \sqrt{\pi}. \qquad (7)$$

We define the wavelet cross-scalogram as

$$E_{XY}(a,t) = W_X^*(a,t)\, W_Y(a,t). \qquad (8)$$

If the analyzing wavelet is complex, the cross-scalogram is also complex and can be written in terms of its real and imaginary parts. The net contribution to the averaged energy is expressed in real values, and we analyze the wavelet co-scalograms, instead of the cross-scalograms.

We take the relation between the second order moment and the wavelet spectrum as

$$\overline{X(t)Y(t)} = \frac{1}{C_\psi} \lim_{T\to\infty} \frac{1}{T} \int_{-\infty}^{\infty} \int_{-T/2}^{T/2} E_{XY}(a,t)\, dt \frac{da}{a^2}. \quad (9)$$

Thus, if we draw the local wavelet spectrum, $(1/a)E_{XY}(a,t)/C_\psi$, onto the scalogram, it corresponds to the Fourier spectrum multiplied by the frequency.

Figures 13 and 14 show the wavelet scalogram in the APG flows with and without the FST, respectively. Irrespective of the pressure gradient without the FST, the mean bursting frequency and the peak location of dissipation spectra correspond to $f' \simeq 0.1$ and $f' \simeq 1$, respectively (Nagano *et al.*, 1998). In the contour maps of Figs. 13 and 14, the interval between successive contour lines is 0.1. The abscissa is the time normalized by the Taylor time scale. The nondimensional time labeled from 300 to 400 correspond to the full time history of waveforms shown in Fig. 8. Thus, Fig. 13 and 14 show a seven times larger time period than that in Fig. 8. It is confirmed that if we integrate the scalograms over the measured time, the global wavelet spectra well correspond to the power spectra shown in Figs. 11 and 12.

As seen from Fig. 13, the contribution from the lower frequency region to the u-fluctuation is observed, whereas that from the higher frequency region to the v-fluctuation is observed. The wavelet scalograms are of intermittent nature. Some local maxima exceed over three times the time-averaged value in the v-fluctuation as shown in Fig. 13(b). If we add the FST, as seen from Fig. 14(a), the contribution from the lower frequency, say 0.005, is enhanced in the scalogram of u-fluctuation. And the local wavelet spectra reveal that the strong interaction, consisting of the near-wall turbulence with high frequency and FST with low frequency, occurs intermittently. On the other hand, as shown in Fig. 14(b) the contribution to the v-fluctuation extends to the higher frequency region.

CONCLUSIONS

Experimental investigation has been made on the effects of the free-stream turbulence (FST) on the turbulent boundary layers subjected to adverse pressure gradients (APG). The results can be summarized as follows:

(1) By imposing the FST, the boundary layer thickness grows rapidly and the mean velocity increases at the same wall-normal distance y/δ. Despite the slight increase in the streamwise turbulence intensity at the outer edge of the boundary layer, the intensity becomes much larger in the middle of the layer, and these tendencies are more evident in the APG flow. On the other hand, the wall-normal velocity fluctuations scarcely increase except at the outer edge of the boundary layer, where $v_{\rm rms}$ is larger than $u_{\rm rms}$ due to the effects of the contraction located downstream of the active grid in the settling chamber.

(2) The absolute value of the third-order moment $\overline{vuv}$ in the outer region increases remarkably in the APG flow with the FST. Thus, the wallward transfer observed in the APG flow is enhanced by imposing the FST. This is because the fractional contribution from the $Q2$-motions is much enhanced in the outer region. However, in the inner region, the effects of the FST are very small.

(3) From the observation of the signal traces of the velocity components, the large amplitude fluctuation from the $Q2$-motions is observed in the outer layer. Moreover, the disparities in the frequencies contributing to the streamwise and wall-normal fluctuations become larger.

(4) The local wavelet spectra of streamwise velocity fluctuations reveal that the strong interaction, consisting of the near-wall turbulence with high frequency and FST with low frequency, occurs intermittently.

REFERENCES

Baskaran, V., Abdellatif, O. E. and Brashaw, P., 1989, "Effects of Free-Stream Turbulence on Turbulent Boundary Layers with Convective Heat Transfer", *Proc. 7th Symp. Turbulent Shear Flows*, pp. 20.1.1–20.1.6.

Batchelor, G. K., 1953, "The Theory of Homogeneous Turbulence", Cambridge University Press.

Blair, M. F., 1983, "Influence of Free-Stream Turbulence on Turbulent Boundary Layer Heat Transfer and Mean Profile Development, Part I - Experimental Data", *Trans. ASME, J. Heat Transfer* Vol. 105, pp. 33–40.

Bradshaw, P., 1967, "The Turbulence Structure of Equilibrium Boundary Layers", *J. Fluid Mech.* Vol. 29, pp. 625–645.

Castro, I. P., 1984, "Effects of Free Stream Turbulence on Low Reynolds Number Boundary Layers", *Trans. ASME, J. Fluid Engineering* Vol. 106, pp 298–306.

Cutler, A. D. and Johnston, J. P., 1989, "The Relaxation of a Turbulent Boundary Layer in an Adverse Pressure Gradient", *J. Fluid Mech.*, Vol. 200, pp. 367–387.

Farge, M., Kevlahan, N., Perrier, V. and Goirand, É., 1996, "Wavelets and Turbulence", *Proc of IEEE*, Vol. 84, pp. 639–669.

Hancock, P. E., and Bradshaw, P., 1983, "The Effects of Free-Stream Turbulence on Turbulent Boundary Layers", *Trans. ASME, J. Fluid Engineering* Vol. 105, pp. 284–289.

Hishida M. and Nagano Y., 1988, "Turbulence Measurements with Symmetrically Bent V-Shaped Hot-Wires. Part 1: Principles of Operation", *Trans. ASME, J. Fluid Engineering*, Vol. 110, pp. 264–269.

Houra, T., Tsuji, T., and Nagano, Y., 2000, "Effects of Adverse Pressure Gradient on Quasi-Coherent Structures in Turbulent Boundary Layer", *Int. J. Heat Fluid Flow* Vol. 21, pp. 304–311.

Ligrani, P. M. and Bradshaw, P. 1987 "Subminiature Hot-Wire Sensors: Development and Use", *J. Phys. E: Sci. Instrum.* Vol. 20, pp. 323–332.

Nagano, Y., and Houra, T., 2002, "Higher-Order Moments and Spectra of Velocity Fluctuations in Adverse-Pressure-Gradient Turbulent Boundary Layer", *Exp. Fluids*, Vol. 33, pp. 22-30.

Nagano, Y. and Tagawa, M., 1988, "Statistical Characteristics of Wall Turbulence with a Passive Scalar", *J. Fluid Mech.*, Vol. 196, pp. 157–185.

Nagano, Y., Tagawa, M. and Tsuji, T., 1993, "Effects of Adverse Pressure Gradients on Mean Flows and Turbulence Statistics in a Boundary Layer", *Turbulent Shear Flows 8.* F. Durst et al., ed., Berlin: Springer, pp. 7–21.

Nagano, Y., Tsuji, T., and Houra, T., 1998, "Structure of Turbulent Boundary Layer Subjected to Adverse Pressure Gradient", *Int. J. Heat Fluid Flow* Vol. 19, pp. 563–572.

Skåre, P. E. and Krogstad, P.-Å., 1994, "A Turbulent Equilibrium Boundary Layer near Separation", *J. Fluid Mech.*, Vol. 272, pp. 319–348.